INSTITUTE OF PHYSICS PUBLISHING MEASUREMENT SCIENCE AND TECHNOLOGY

Meas. Sci. Technol. **18** (2007) 131–137 doi:10.1088/0957-0233/18/1/016

Simple techniques for generating nanosecond blue light pulses from light emitting diodes

Omar Veledar[1], Phillip O Byrne[1], Sean Danaher[1], Joseph I H Allen[1], Lee F Thompson[2] and John E McMillan[2]

[1] School of Computing, Engineering and Information Sciences, Northumbria University, Newcastle upon Tyne, NE1 8ST, UK
[2] Department of Physics and Astronomy, University of Sheffield, Sheffield, S3 7RH, UK

E-mail: sean.danaher@northumbria.ac.uk

Received 13 June 2006, in final form 3 October 2006
Published 30 November 2006
Online at stacks.iop.org/MST/18/131

Abstract
The electronic drive requirements for producing nanosecond optical pulses from blue light emitting diodes are considered. Simple circuits are used to generate the fast current pulses necessary to switch on and assist with the turn off of these devices. The intensity of the emitted radiation can be controlled by the magnitude of the drive current. Optical pulses in the nanosecond range are suitable for, but not limited to, the calibration of scintillation counters. The circuits described can be either free running or externally triggered. Typically, the optical pulse full width half maximum (FWHM) is below 1 ns. The presented techniques are not limited to blue LEDs and should be applicable to devices of longer wavelengths.

Keywords: light emitting diode, LED, blue, optical pulse, driver, nanosecond, complementary pair, regenerative switch, PMT, scintillator calibration

(Some figures in this article are in colour only in the electronic version)

1. Introduction

Development of low cost high-speed light emitting diodes (LEDs) that are easy to drive has made them convenient to use as pulsed light sources. The optical spectrum they cover is from the ultraviolet (UV) to the infrared (IR), but this work is confined to blue emitting LEDs. Their ability to generate very fast light pulses is often exploited in complex optical systems. A common example is their use for calibration of scintillation counters and photomultiplier tubes (PMT) [1–5]. Various concepts have been employed for the creation of optical pulses using LEDs [6]. Some early optical pulse generators successfully utilized the switching speed of the avalanche transistor to produce fast current pulses to activate LEDs [5, 7]. Complementary transistors, configured as a regenerative switch, which operate at a nanosecond range offer an alternative method of achieving very fast switching times. Kapustinsky *et al* [8] used this technique to produce optical pulses needed to calibrate the scintillation counters and PMT arrays.

We have further developed and improved the switching times of the regenerative switch and modified it so that it can be either free running or triggered on the negative edge of a trigger pulse. Efforts to empirically match the dynamic impedance of the LED to the output characteristics of the switch were evaluated. Various coupling and matching circuits from the switch were developed; the choice of output circuitry depends on the application. The fundamental configuration of the switching circuit is, however, the same in all cases.

The blue LED light source used is housed in a standard 5 mm diameter plastic package and has a stated optical emission at 472 nm [9]. Measurements were made on a number of LEDs to establish the manufacturing range of their physical characteristics. A peak emission wavelength was also experimentally confirmed for these devices. These data are used in the design of the electronic circuitry. The spread of

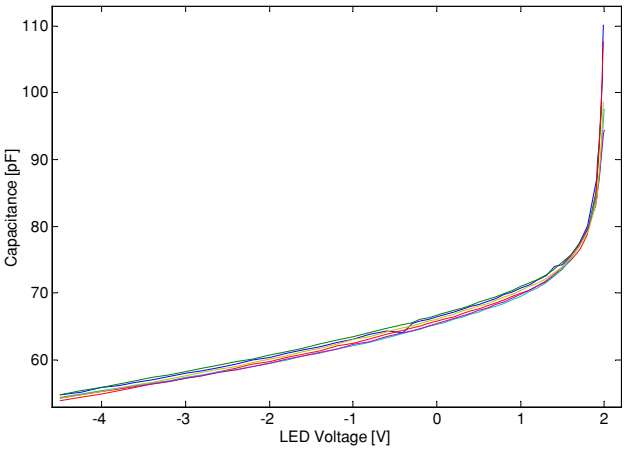

Figure 1. LED capacitance–voltage characteristics.

the physical characteristics was taken into account to ensure consistency of the drive current and optical output. The designed electronic circuits produce repeatable and reliable optical pulses with a FWHM of below 1 ns.

We have concentrated on the use of the blue LEDs because they are appropriate for our particular application. Blue LEDs are among the most difficult LEDs to optically pulse because of their large energy bandgap and high internal capacitance. This leads to an assumption that our techniques should be applicable to LEDs emitting at longer wavelengths. We have preliminarily checked this assumption by applying our techniques to inexpensive 'off the shelf' 5 mm and 3 mm green, yellow and red LEDs. The devices generate fast optical pulses as expected.

2. LED characteristics

The rise time, fall time and pulse width of the generated optical signal is ultimately dominated by the physical characteristics of the LED itself. Instantaneous switching between the on and off states is not possible to achieve. When a p–n junction is forward biased and current flows, minority carriers are injected into both sides of the junction. This disturbance of the thermal equilibrium initiates the start of the recombination process, which generates the optical output. The time the carriers take to travel across the depletion region, together with the time carriers take to recombine, represents a delay between the stimulating current pulse and optical output. When the electrical signal to the junction is removed the excess minority carriers contained within the junction take a finite time to recombine with the majority carriers. Thus they are responsible for the exponential turn-off decay [10].

Figure 1 shows the combined depletion and diffusion capacitance plotted against bias voltage for six of the blue LEDs studied in the experiment. When the diode starts to conduct, the depletion capacitance disappears and the finite time of the injected carriers causes the diffusion capacitance. Figure 2 depicts a simple equivalent circuit of the LED where R_s and R_p are series and parallel resistances respectively and C is the diode capacitance consisting of the sum of junction and diffusion capacitance. The dynamic electrical impedance presented by the diode during switching is that of

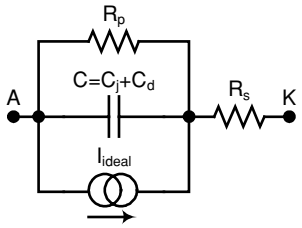

Figure 2. Basic LED model.

a complex voltage-dependent impedance, initially dominated by the depletion capacitive reactance in parallel with a high resistance. At forward bias voltages greater than about 1 V the impedance is controlled by the diode equation (equation (1)) in parallel with diffusion capacitance. The stored charge that causes this capacitance is proportional to the excess minority carrier lifetime. This diffusion capacitance is the dominant factor in the switching speed of the devices [11].

$$I = I_s \left\{ \exp\left[\frac{q\,(V - IR_s(V))}{nkT} \right] - 1 \right\} + \frac{V - IR_s(V)}{R_p(V)}. \qquad (1)$$

The expression shown in equation (1) is used to describe the relationship between the diode current and its voltage where I_s is the diode saturation current, q is the elementary charge, n is the diode ideality factor which takes into account the continuous generation–recombination process inside the diode depletion layer, k is Boltzmann's constant and T is temperature. This expression also accounts for the voltage drop across the diode series resistance $R_s(V)$ and the current through the parallel resistance $R_p(V)$. The second term in the expression represents the current flowing through the parallel resistance, which normally has negligible contribution in forward bias.

The LED frequency response is also defined by the ratio of the forward to reverse currents [12, 13] and the additional parasitic capacitance [11].

The frequency response of the LEDs can be improved by reducing the minority carrier lifetime. This can be achieved by the insertion of recombination–generation centres that have energy levels located near the mid gap of the material forming the p–n junction, such as gold in silicon. The reduction of the minority carrier lifetime is however inevitable in highly doped active regions or in heterostructures. The minority carrier lifetime is reduced in heterostructures by the formation of high carrier concentrations within small well regions [14]. The reduction of minority carrier lifetime inevitably results in the decline of LED quantum efficiency. Therefore, this is not such a feasible solution for the applications that require maximum possible optical output.

The frequency response of an LED is given by equation (2) providing that the low-level injection conditions are satisfied. The minority carrier lifetime τ_c defines the LED frequency response as shown in equation (2) where $R(f)$ is the response at a given frequency f. For the high-level injection the concept of constant lifetime no longer applies and some average value of τ_c must be assumed [15]:

$$R(f) = \frac{R(0)}{\sqrt{1 + 4\pi^2 f^2 \tau_c^2}}. \qquad (2)$$

The series resistance, R_s, is a combination of the resistance of the neutral regions and the internal contact resistance [14].

The value of R_s for a particular diode can be established from equation (3) in conjunction with the manufacturer's published data. The derivative needs to be taken at voltages significantly larger than the diode threshold voltage where the slope of the I–V curve is relatively constant:

$$R(V) = \frac{\mathrm{d}V}{\mathrm{d}I}. \tag{3}$$

Ideally the series resistance should be zero, but in practice the LEDs we use exhibit series resistance in the region of 30 Ω.

The parallel resistance, R_p, is the result of any conduction channel that bypasses the p–n junction. This is normally a consequence of damaged regions and surface imperfections [14]. To find the value of the parallel resistance the relationship shown in equation (3) is also valid. In this case the derivative is measured in the reverse bias section of the I–V characteristic. Ideally the parallel resistance should be infinitely high. The parallel resistances of the LEDs employed in this case are of the order of 22 MΩ. This resistance controls the slope of the diode I–V characteristic in the reverse bias region. It also affects the slope of the same curve at low forward bias voltages where the value of the parallel resistance is comparable to the diode dynamic resistance.

The junction capacitance per unit area for a p–n junction is defined in equation (4) [10], where dQ is the incremental change in the depletion layer charge per unit area due to an incremental change in the applied voltage dV. This capacitance is caused by the 'parallel plate effect' formed by the depletion layer within the p–n junction. This capacitance is dominant in reverse bias and at low forward bias where its value increases because the 'effective plate gap' is reduced. Once the diode starts to conduct, the junction capacitance is destroyed. Accurate modelling of the junction capacitance in this transition region is somewhat difficult to achieve [16, 17].

$$C(V) = \frac{\mathrm{d}Q}{\mathrm{d}V}. \tag{4}$$

The diffusion capacitance appears once the diode starts to conduct. This capacitance is a result of the charge storage in the p–n junction caused by the minority carrier distribution [10]. The amount of stored charge is the product of the current and the minority carrier lifetime [10]. Equation (4) also represents the diffusion capacitance. This capacitance becomes dominant when the diode is forward biased. The diffusion capacitance is negligible when the diode is reversed biased because few excess minority carriers are present in the junction. This diffusion capacitance plays a dominant role in controlling the switching speed of the devices [11].

It is generally considered a good practice when operating an LED to reverse bias the junction after the drive pulse is removed in order to remove from the active region the remaining excess minority carriers that have not managed to recombine. This technique markedly reduces the 'turn-off' delay. This latter point is studied in this paper for a given range of currents.

3. Experimental methods

The developed circuitry relies on the use of a cross-coupled pair of complementary transistors. The transistors are concurrently in either a hard 'off' or 'on' state due to positive feedback. This combination provides a quiescent current of almost zero while its on state provides a high current capability. The base currents of the transistors are derived from the collector current of their counterpart so that the current rating is uniquely determined by the transistor ratings [18].

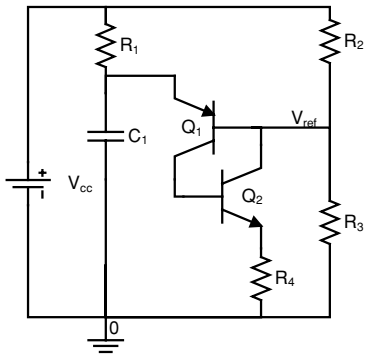

Figure 3. Basic complementary pair regenerative switch configuration.

3.1. Regenerative switch

The basic free-running relaxation oscillator circuit is shown in figure 3. Consider initially that C_1 is uncharged and hence has a zero voltage across it. Transistors Q_1 and Q_2 are both in the off state. The potential V_{ref} is then defined by the potential divider formed by R_2 and R_3. Capacitor C_1 charges through R_1. When the voltage across this capacitor exceeds V_{ref} by the amount of base–emitter voltage of transistor Q_1 the same transistor starts to conduct. This turns on Q_2 which causes V_{ref} to fall quickly turning Q_1 fully on. This action provides a low impedance path for capacitor C_1 to discharge through R_4 causing the regenerative switch to return to its initial condition. The free-running period is controlled by the time constant R_1C_1 and the magnitude of V_{ref}. The rise time of the output pulse developed across R_4 is a function of the switching speeds of Q_1 and Q_2 while the turn-off time is dictated by the discharge current path formed by Q_1, Q_2, R_4 and the value of C_1.

Figure 4 shows a free-running circuit with component values designed to produce pulses with a rise time of 2.9 ns at a repetition frequency of 23 kHz. The component values (especially C_1) are chosen to optimize the speed of the pulses. The repetition rate is arbitrary and is determined by R_1, R_2, R_3 and C_1. By varying the supply voltage, V_{CC}, a family of output curves (measured across R_4) can be produced as shown in figure 5 where the curves A–E correspond to different supply voltages. The ringing on the graph is thought to be caused by parasitic impedance and non-uniform impedance mismatch of the probe cable. Capacitor C_2 provides a small amount of feedback which enhances the initial 'turn-on' time of the pulse. The values of C_3 and R_4 have been established empirically to give optimum results when driving an Agilent blue LED of type HLMP-CB15 [9] and the pulse forming network attached to the circuit board between points X and Y.

By removing R_3 and connecting a capacitor C_t to point V_{ref} the device can be externally triggered by a negative pulse. The points X and Y in figure 4 are the positions where the LED and its associated pulse forming network are connected.

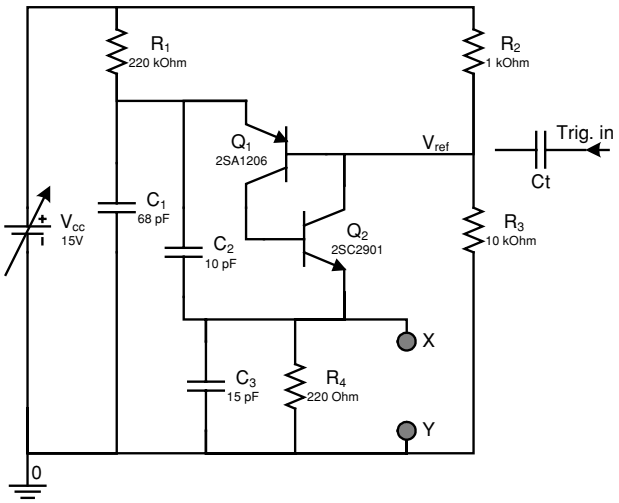

Figure 4. Standard driver configuration.

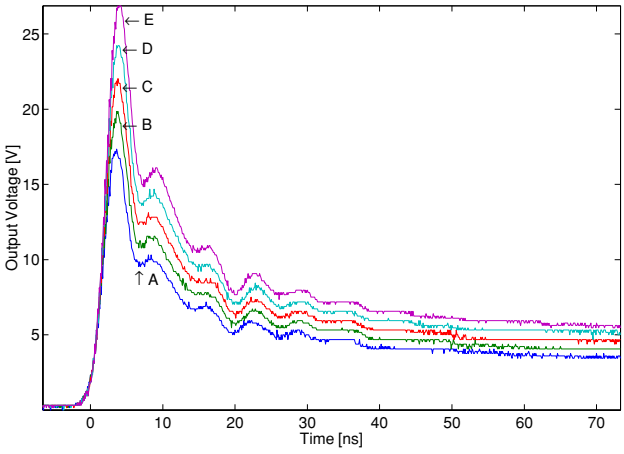

Figure 5. Regenerative switch output.

3.2. Pulse shaping circuits

Diode pulse shaping is achieved by using fast signal diodes (e.g., Philips 1N4148). These diodes are characterized by a fast recovery time, typically 4 ns, and a very low diode capacitance of 4 pf at zero bias voltage, whereas the LED has a measured depletion capacitance of over 66 pF at zero volts (figure 1). Figures 6(*a*)–(*d*) illustrate the four pulse shaping circuits considered. In each case, the points X and Y correspond to those in figure 4. By incorporating two diodes in a simple circuit, figure 6(*a*), the inherent output of the regenerative switch is modified. The LED drive voltage rise time is dictated by the switching speed of the regenerative switch but the fall time is controlled by R_5 in series with D_2. The LED initially conducts and then the diode D_2 clamps the drive signal to ground. The inclusion of D_1 in the circuit sharpens the turn on step. The magnitude of resistor R_5 can be used to alter the time response of diode D_2. Hence, it affects the amount of energy delivered to the LED. The switching-off action of the LED is controlled actively, but the device is not driven into reverse bias upon removal of the driving pulse.

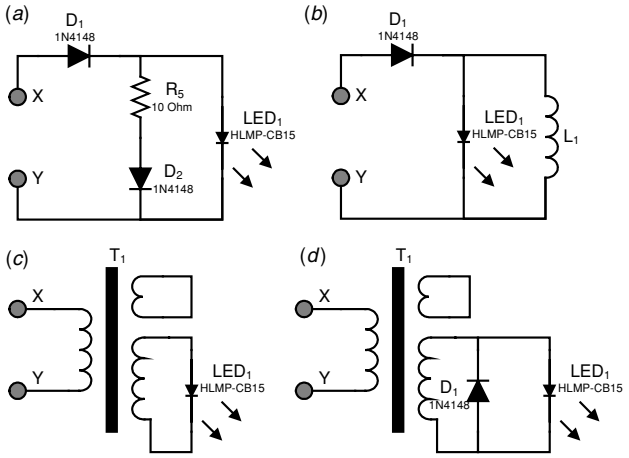

Figure 6. Pulse shaping and LED coupling configurations: (*a*) switching diode shaping, (*b*) carrier sweep out, (*c*) shorted turn and (*d*) shorted turn clipped.

In figure 6(*b*), a small inductor L_1 is placed in parallel with the LED forming a resonant circuit. This allows the voltage across the LED to swing negative. Its shape is controlled by the amplitude of the initial pulse and the voltage dependence of the depletion capacitance of the LED. In general terms it is a damped oscillator. L_1 is constructed from six turns of 0.54 mm diameter enamel covered copper wire wound on a 5 mm diameter former. The coil is self-supporting on the circuit board. It has the value of 0.19 μH measured at 100 kHz.

The transformer in the circuit figure 6(*c*) is fabricated by bifilar winding three turns of 0.54 mm enamel coated copper wire on a torodial former (Ferroxcube, type TN9/6/3-4C65). An additional two turns of the same type of wire are placed centrally and directly on top of these windings. These additional turns are shorted together. This configuration forms a pulse transformer whose self-inductance is 0.50 μH measured at 100 kHz. A pulse transformer with shorted turns effectively differentiates the input drive pulse. This is caused by the prompt collapse of the magnetic flux within the ferrite core due to the influence of the shorted turns which act as a very low impedance secondary winding. The result of this action is a rapid negative swing. At the operational frequency of the circuit, the physical properties of the ferrite core are at the upper limits of their specification. On the negative swing of the drive voltage the waveform is a function of the inductance of the transformer and the LED capacitance. Modifying this circuit by the inclusion of a clamping diode D_1, figure 6(*d*), restricts the negative swing and subsequent overshoot.

3.3. Measurement techniques

The photomultiplier tube (Hamamatsu R7400U) and its associated circuitry are housed in a small metal box (Hamamatsu H6780 PMT module). Typical rise time and electron transit times for the PMT are 0.78 ns and 5.4 ns, respectively. A coupling assembly is used to interface light sources to the optical window of the photomultiplier tube. The LED is held 4 mm from the optical window. The gain of the PMT is controlled by a potentiometer which allows the

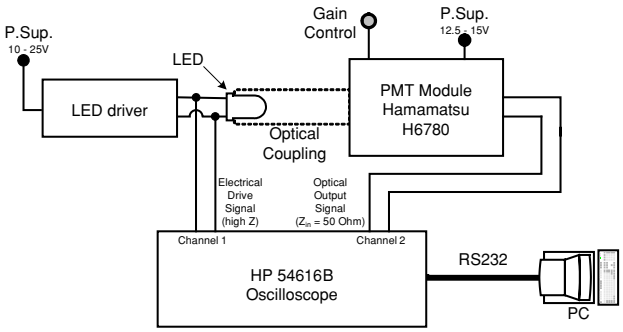

Figure 7. Experimental configuration.

output voltage of the PMT to be adjusted and maintained at a constant level for a wide range of optical intensities. Figure 7 is a schematic showing the equipment layout used for evaluation of the drive and optical pulses. Data were collected and stored in a spreadsheet using Agilent IntuiLink 54600 software. MATLAB is used for data plotting.

4. Results and discussion

The narrowest pulses achieved experimentally without pulse shaping have 5 ns FWHM. The minimum voltage required to stimulate light production using such driving pulses is 5.2 V. When the oscilloscope probe was connected to the circuit, this condition was satisfied for a V_{cc} of 15 V. The amplitudes of all of the LED drive pulses are controlled by varying the magnitude of V_{cc} in three steps of 2 V from the point when the circuit starts generating an optically significant signal. This corresponds to a drive voltage of 12 V for the circuit in figure 6(*a*), 13 V for the circuit in figure 6(*b*) and 17 V for the circuits in figures 6(*c*) and (*d*). Figures 8(*a*)–(*d*) show the measured input drive signal and the observed optical signal for the four circuits illustrated in figures 6(*a*)–(*d*). In each figure the curves A–D correspond to first optically significant signal (A), +2 V (B), +4 V (C), +6 V (D).

From figure 8(*a*), it can be seen that a simple diode pulse shaping technique can produce a well-defined LED driving pulse. By altering V_{cc} over the stated range of voltages, the current flowing through the LED is altered accordingly. Curve A in the lower half of figure 8(*a*) shows a well-defined optical pulse which closely mirrors the drive pulse shown in the upper part. The delay between the two pulses is caused by the time taken to produce the optical pulse and the electron transit time of the PMT. As the drive voltage is increased there is a corresponding increase in the decay time of the optical pulse, B, C and D. Higher drive voltages inject more carriers into the LED. The recombination time taken for these to be neutralized by a fixed number of photon producing traps within the fabric of the LED is also increased; hence longer decay times are seen in the optical pulse.

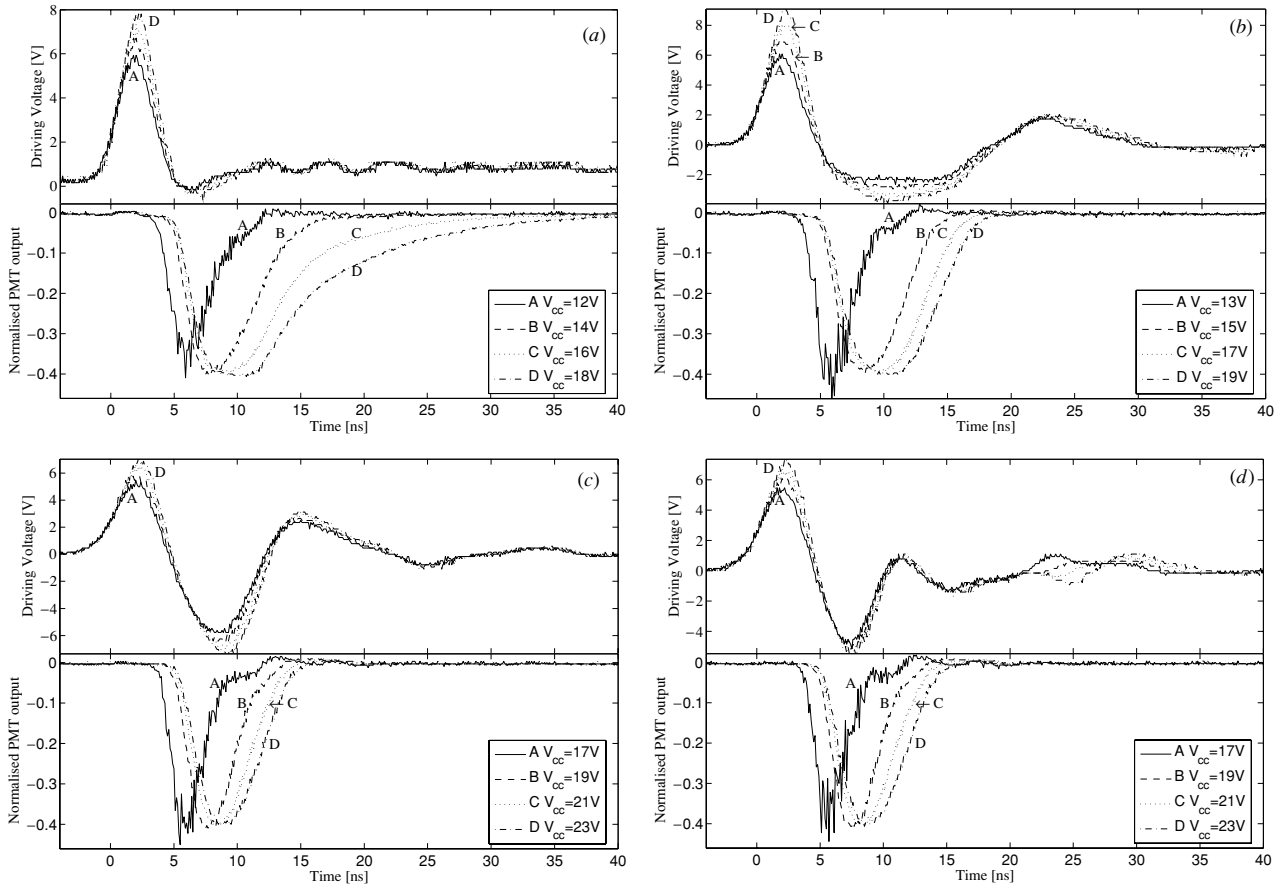

Figure 8. LED driving and optical output signals: (*a*) diode shaping, (*b*) inductive swing, (*c*) shorted turn and (*d*) clipped shorted turn.

Table 1. Timing results—as measured.

Circuit and curve	Time	Best—plot A Electrical time (ns)	Best—plot A Optical time (ns)	Worst—plot D Electrical time (ns)	Worst—plot D Optical time (ns)
6(*a*)	Rise	2.24	2.12	2.04	1.91
and	FWHM	3.45	3.81	3.56	13.90
8(*a*)	Fall	3.10	3.80	2.96	34.29
6(*b*)	Rise	2.04	1.75	2.07	1.85
and	FWHM	3.28	3.27	3.22	8.73
8(*b*)	Fall	2.37	2.23	2.05	9.62
6(*c*)	Rise	2.07	1.65	1.99	1.91
and	FWHM	3.79	3.14	3.80	4.36
8(*c*)	Fall	1.96	1.87	1.80	3.99
6(*d*)	Rise	3.07	1.85	3.01	2.00
and	FWHM	3.69	3.02	3.67	6.23
8(*d*)	Fall	1.88	2.21	1.81	5.97

In figure 8(*b*) it can be clearly seen that swinging the drive voltage negative significantly reduces the decay time of the optical pulse. In effect, this technique removes the excess carriers from the LED's active region. This is analogous to discharging the diffusion capacitance of the LED. The negative portion of the drive pulse is slow to reach its maximum voltage and has an extended duration of 2.5 times that of the drive pulse. This shape is not optimal for the efficient removal of the excess carriers.

A transformer with shorted turns (figure 8(*c*)) effectively differentiates the input drive pulse. This is caused by the magnetic flux within the ferrite core collapsing quickly. A rapid negative swing results from this action. It can be seen from this graph that the optical decay occurring within the LED is markedly improved. Again, the changing depletion capacitance affects the negative waveform. A problem with this basic circuit is that the negative voltage swing can exceed the reverse breakdown voltage of the LED.

The final circuit (figure 6(*d*)) uses a 1N4148 switching diode to restrict the magnitude of the negative swing by clamping. Its effect can clearly be seen in figure 8(*d*). While the optical output curves of this figure are similar to those shown in figure 8(*c*), the danger of electrical damage to the LED has been reduced.

The measurements of both the electrical and optical 10–90% rise times, FWHM and 90–10% fall times were made from data used to plot figures 8(*a*)–(*d*) and are shown in table 1. Only the best (plot A) and worst (plot D) parameters have been tabulated for the various pulse forming circuits, figures 6(*a*)–(*d*). It can be observed that in all cases the positive component of the drive voltage has similar timing characteristics. In the simple circuit (figure 6(*a*)) it can be readily seen that for a low LED drive voltage (hence current) the optical pulse closely follows the stimulating voltage. The delay between the drive voltage and the optical pulse is the time taken for the blue LED to produce its optical signal and be detected by the PMT. The light generation is dictated by the structure of the device and the quantum processes involved. At higher drive voltages (larger currents) the time for the excess carriers to recombine with the fixed number of traps within the semiconductor junction extends the optical decay time.

By allowing the drive voltage to swing negative (figure 8(*b*)) the excess carriers can, to some extent, be removed from the active region thus speeding up the optical pulse. The simple inductive circuit used to achieve this, figure 6(*b*), has a slow negative time response and as such is inefficient in carrying out this task. Circuits figure 6(*c*) and (*d*) and their corresponding graphs show a fast-falling negative component in the drive pulse and this is reflected in well-defined and much quicker optical signals.

4.1. Measurement errors

It should be noted that the oscilloscope probes used in this work have an input capacitance of 10 pf. When a measuring probe was connected to the regenerative switch and LED combination, it loaded the circuit reducing the drive power to the LED. Throughout all the measurement of drive voltages, the same probe was coupled to the LED leads but no effect was observed on pulse shape or timing. The optical output measurements were made from the PMT module with the scope set to 50 Ω input impedance. No oscilloscope probe is used for the measurement of the optical pulse.

The timing results presented in table 1 do not take into account the limitations in performance of the PMT module and oscilloscope. For measurement systems which use two or more independent components the errors add in quadrature [19]. The rise times of the oscilloscope and the PMT are 0.7 ns and 0.78 ns, respectively. Hence, the rise time of the system is defined by equation (5):

$$\tau_r = \sqrt{(0.7\,\text{ns})^2 + (0.78\,\text{ns})^2} \approx 1\,\text{ns}. \tag{5}$$

Assuming that the fall time of the PMT is typically twice the rise time, the fall time of the system is defined in equation (6):

$$\tau_f = \sqrt{(0.7\,\text{ns})^2 + (1.56\,\text{ns})^2} \approx 1.7\,\text{ns}. \tag{6}$$

A general approximation of the FWHM being equal to the sum of the rise and fall times of the system yields an approximate value for the system FWHM of 2.7 ns. This is the response of the system to a delta function light flash. This

Table 2. Best-achieved timing results.

Circuit and curve	t_{rise} (ns)	FWHM (ns)	t_{fall} (ns)
6(*a*) and 8(*a*) (A)	1.04	2.73	4.23
6(*b*) and 8(*b*) (A)	1.04	2.20	2.76
6(*c*) and 8(*c*) (A)	0.73	1.31	2.22
6(*d*) and 8(*d*) (A)	0.80	0.74	2.10

response degrades the observed FWHM according to equation (7) which can thus be used to calculate the optical FWHM.

$$\mathrm{FWHM}_{\mathrm{optical}} = \sqrt{(\mathrm{FWHM}_{\mathrm{observed}})^2 - (\mathrm{FWHM}_{\mathrm{system}})^2}. \quad (7)$$

The calculated timing characteristics of the best-achieved optical signals are listed in table 2.

The measurements are repeated using a LeCroy (waveRunner 6100 1 GHz) oscilloscope with the typical rise time of 0.4 ns. The calculated timing characteristics of optical signals from the repeated measurements are in agreement within experimental error with the results shown in table 2.

One possible alternative method for evaluating the timing characteristic of the generated light flashes employs the single photon technique [20]. This procedure requires two PMTs. One PMT, which collects a large amount of light from the flashing device, provides a zero-time signal by sensing the formation of the first few photoelectrons at its cathode. The other PMT is set in such a way that its probability of photon detection per pulse is much lower than unity. The pulse shape is determined by constructing a histogram of the time differences between two PMT signals over many flashes. This technique is more accurate and with typical components generates a FWHM accuracy of approximately ± 100 ps [21].

5. Conclusion

A simple regenerative switch using complementary transistors used in conjunction with simple pulse shaping circuits can produce extremely fast pulses. We demonstrate that these pulses are suitable for producing fast optical signals from LEDs. Taking into account measurement errors a FWHM time of below 1 ns has been achieved. At higher drive currents simple inductively generated negative transients successfully sweep out the excess carriers from the junction. This allows higher intensity blue flashes to be generated. The simplicity of the circuits used allows them to be either free running or externally triggered for synchronization purposes.

Acknowledgments

The authors wish to express their thanks to A Scott, K Williams, T Caisley, P Donnelly and J Bagnall of Northumbria University for their technical assistance; Mark5 Ltd for their assistance with transistor samples. The authors are exceptionally grateful to Professor Alistair Sambell, Dean of School of Computing, Engineering and Information Sciences of Northumbria University, for general comments and support on the project.

References

[1] Amram P *et al* (for the ANTARES collaboration) 2002 The ANTARES optical module *Nucl. Instrum. Methods Phys. Res.* A **484** 369–83
[2] Sefzick T, Kilian K, Oelert W and Wienands G 1990 A system for simulation of scintillator light signals *Nucl. Instrum. Methods Phys. Res.* A **288** 571–3
[3] Reiter W L and Stengl G 1981 A blue light emitting diode used as a reference element in scintillation spectrometers *Nucl. Instrum. Methods* **180** 105–57
[4] Reiter W L and Stengl G 1980 A long term stable reference light source using LEDs for stabilisation of scintillation spectrometers *Nucl. Instrum. Methods* **173** 275–82
[5] Green D R 1978 A LED system to test scintillation counter hodoscopes *Nucl. Instrum. Methods* **151** 307–12
[6] Veledar O, Danaher S, Allen J I H, Byrne P O and Thompson L F 2005 Review and development of nanosecond pulse generation for light emitting diodes *Scientific Reports, J. University of Applied Sciences Mittweida (Wissenschaftliche Berichte, Wissenschaftliche Zeitschrift der Hochschule Mittweida (FH))* **9/10** 3–6
[7] Samueli J J and Sarazin A 1964 A nanosecond pulse generator and shaping circuit with avalanche transistors *Nucl. Instrum. Methods* **26** 71–6
[8] Kapustinsky J S, DeVries R M, DiGiacomo N J, Sondheim W E, Sunier J W and Coombes H 1985 A fast timing light pulser for scintillation detectors *Nucl. Instrum. Methods Phys. Res.* A **241** 612–3
[9] Agilent Sun Power Series HLMP-CB15 InGaN Blue Lamp
[10] Sze S M 2002 *Physics of Semiconductor Devices* 2nd edn (New York: Wiley)
[11] Liu J M 2005 *Photonic Devices* (Cambridge: Cambridge University Press)
[12] Millman J and Taub H 1965 *Pulse, Digital and Switching Waveforms—Devices and Circuits for Their Generation and Processing* (New York: McGraw-Hill)
[13] Kingston R H 1954 Switching time in junction diodes and junction transistors *Proc. IRE* **42** 288–93
[14] Schubert E F 2003 *Light Emitting Diodes* (Cambridge: Cambridge University Press)
[15] Wilson J and Hawkes J 1998 *Optoelectronics—An Introduction* 3rd edn (London: Prentice Hall Europe)
[16] Chawla B R and Gummel H K 1971 Transition region capacitance of diffused p-n junctions *IEEE Trans. Electron Devices* **18** 178–95
[17] Massobrio G and Antognetti P 1993 *Device Modelling with SPICE* 2nd edn (New York: McGraw-Hill)
[18] Littauer R 1965 *Pulse Electronics* (New York: McGraw-Hill)
[19] Johnson H W and Graham M 1993 *High Speed Digital Design; a Handbook of Black Magic* (Englewood Cliffs, NJ: Prentice Hall)
[20] Bollinger L M and Thomas G E 1961 Measurement of the time dependence of scintillation intensity by a delayed-coincidence method *Rev. Sci. Instrum.* **32** 1044–50
[21] McMillan J E 1999 The single photon technique for measuring LED pulser flash width *Sheffield Particle Astrophysics* (Sheffield: Department of Physics and Astronomy Internal Publication, Sheffield University)